JOURNAL OF MATERIALS SCIENCE 21 (1986) 1027–1036

Room-temperature tensile behaviour of bronze-processed multi-filamentary Nb_3Sn superconducting materials

SHOJIRO OCHIAI, KOZO OSAMURA
Department of Metallurgy, Kyoto University, Kyoto 606, Japan
TOSHIHIRO UEHARA
Graduate School, Kyoto University, Kyoto 606, Japan

Structure and its relation to fracture behaviour of multi-filamentary Nb_3Sn superconducting composite materials prepared by the bronze method were studied by tensile testing at room temperature. There were two types of fracture mode. Type I showed high elongation, accompanied by apparent plastic deformation of composites as a whole and the Nb_3Sn layer exhibited multiple fracture. Type II showed no apparent plastic deformation and the composites fractured in a brittle manner. Type I occurred when the fraction of the Nb_3Sn layer was small and the drop of load-bearing capacity due to fracture of Nb_3Sn layer could be compensated mainly by strain hardening of ductile constituents of Nb, Cu–Sn and Cu. On the other hand, Type II occurred when the fraction of Nb_3Sn layer was large and the fracture of the Nb_3Sn layer caused fracture of composites as a whole. To describe the tensile strength of composites for both types, a model was proposed, which explained well the experimental results. It was found that the strength of the Nb_3Sn layer decreases with increasing diameter of composites and with increasing annealing temperature and time.

1. Introduction

Superconducting materials are subjected to high mechanical stresses arising from winding tension and bending strain during fabrication, differential thermal contraction between different materials in the magnetic structure and the Lorenze force when a magnet is energized, as pointed out by Ekin [1]. Under these high stresses, the lack of ductility of the Nb_3Sn compound has serious consequences for handling. Thus it is very important to know the deformation-behaviour and fracture behaviour of this compound and its relation to the behaviour of composites as a whole. Up to date, much effort has been made to clarify the mechanical behaviour of superconducting composite materials, including the pre-strain effects on superconducting characteristics [1–8]. The fracture behaviour of Nb_3Sn compound in composites has, however, not been investigated for a wide variety of factors such as specimen size, annealing temperature and time. The aim of the present work is to investigate the tensile behaviour of superconducting composite materials by changing the above factors and to obtain fundamental information on this subject.

2. Experimental procedure

The specimens employed in the present study were the multi-filamentary composites supplied as the Japanese standard reference samples for energy research programmes in 1983–1985 of the Ministry of Education, Science and Culture of Japan. Three kinds of composite specimen were used in this study. The only difference between these was the diameter of composites as a whole, d_c(0.31, 1.02 and 2.60 mm). In this work, composites with d_c = 0.31, 1.02 and 2.60 mm are called as S1, S2 and S3, respectively. All composites were composed of 745 niobium filaments in Cu–13 wt% Sn alloy, surrounded with a niobium barrier and then pure copper as a stabilizer, as shown in Fig. 1 where the cross-section of the S1 specimen is presented as an example. The bronze and copper to non-copper ratios were 2 and 0.445, respectively, in all kinds of composites. The average diameter of the niobium filaments, d_f, and the thickness of the niobium barrier, c_b, of as-supplied samples measured at the authors laboratory are shown in Fig. 2. Both d_f and c_b are proportional to d_c, indicating that the S1 to S3 specimens are geometrically similar.

Two series of experiments were carried out. In one series (Experiment 1), the S1 to S3 samples were annealed at 973 and 1073 K for 432 ksec in vacuum, which will clarify the effects of specimen size on structure and tensile behaviour. In another series (Experiment 2), the S3 specimens were annealed isothermally at 973 and 1073 K for various periods of time, which will clarify the effects of annealing temperature and time on structure and tensile behaviour. After annealing, all specimens were embedded in resin and the cross-sections were polished. Using the polished cross-sections, the thickness of the Nb_3Sn layer and volume fractions of Nb_3Sn, Nb and Cu–Sn were measured with a scanning electron microscope (SEM) and the tin concentration in the Cu–Sn matrix was measured

0022–2461/86 $03.00 + .12

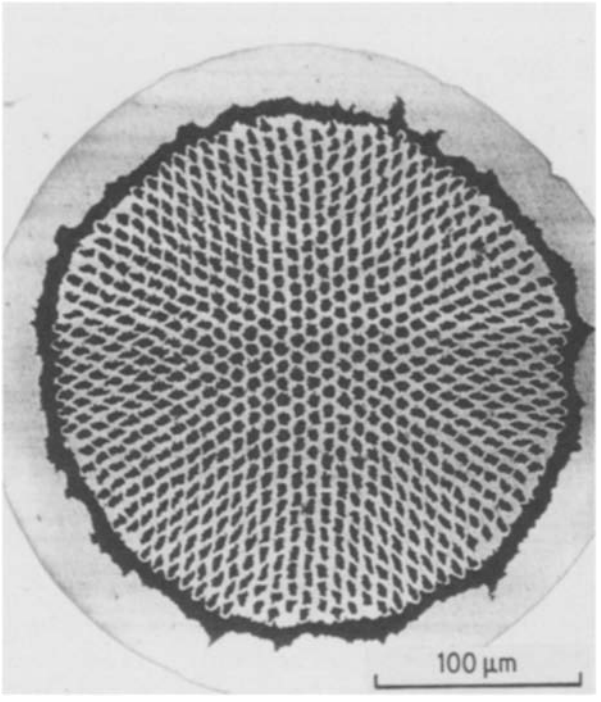

Figure 1 Cross-section of the S1 specimen.

with electron probe microanalysis (EPMA) followed by the ZAF correction. Tensile testing was carried out with an Instron type tensile machine at room temperature at a strain rate of $3.33 \times 10^{-3}\,sec^{-1}$. The fractured specimens were observed using a SEM.

3. Results

3.1. Structure of annealed specimens

3.1.1. Experiment 1

After annealing at 973 and 1073 K for 432 ksec, the tin concentration in the Cu–Sn matrix, x_{Sn}, the thickness of Nb_3Sn layer, c, the volume fraction of Nb_3Sn which is the sum of the volume fractions of Nb_3Sn formed on niobium filaments and at the niobium barrier, V_{Nb_3Sn}, and that of niobium which is the sum of the volume fractions of niobium filaments and the niobium barrier remaining after reaction, V_{Nb}, were measured, as shown in Table I. As the copper to non-copper ratio was 0.445, the volume fraction of copper, V_{Cu}, was 0.308, which did not vary with heat-treatment. The volume fraction of Cu–Sn, V_{Cu-Sn}, was calculated from the equation $1-V_{Nb_3Sn}-V_{Nb}-V_{Cu}$. As shown in Table I, the larger the d_c, the higher the x_{Sn}, c, V_{Cu-Sn} and V_{Nb}, but the lower the V_{Nb_3Sn}. This tendency was more predominant for the annealing temperature,

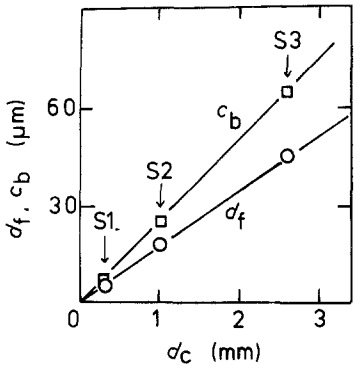

Figure 2 Average measured values of d_f and c_b plotted against d_c.

$T = 1073$ K. Under the present annealing treatment for a given period of 432 ksec, almost all elemental tin has reacted with niobium, forming Nb_3Sn in the S1 specimens but not in the S2 and S3 specimens. However, c in S2 specimens was larger than that in S1 specimens, and c in S3 specimens was larger than that in S2 specimens, at both T = 973 and 1073 K. This results from the difference in d_c in the fact that available elemental tin which forms Nb_3Sn is present to a greater extent in thicker specimens than in thinner specimens for one filament, since the original structures of S1 to S3 specimens were geometrically similar.

3.1.2. Experiment 2

The variations of x_{Sn}, c, V_{Nb_3Sn}, V_{Nb} and V_{Cu-Sn} were also investigated for the S3 specimens annealed at 973 and 1073 K as a function of annealing time, t. The x_{Sn} decreased with increasing t and, accordingly, c increased as shown in Fig. 3. The variations of V_{Nb_3Sn} and V_{Nb} are presented in Fig. 4. The V_{Nb_3Sn} increased but the V_{Nb} decreased with increasing t. The decrease in V_{Cu-Sn} with increasing t was very small (e.g. 0.38 for 43.2 ksec and 0.36 for 1730 ksec at $T = 1073$ K).

3.2. Tensile behaviour of specimens

3.2.1. Experiment 1

Fig. 5 shows the typical stress–strain curves of S1 to S3 specimens annealed at (a) 973 and (b) 1073 K. From the shape of the stress–strain curves, two types of fracture behaviour were found. Type I showed apparent plastic deformation of composites as a whole. The S2 and S3 specimens annealed at 973 K and the S3 specimens annealed at 1073 K showed this type. Type II showed no apparent plastic deformation of composites as a whole. The S1 specimens annealed at 973 K and the S1 and S2 specimens annealed at

TABLE I Average values of x_{Sn}, c, V_{Nb_3Sn}, V_{Nb} and V_{Cu-Sn}, where each specimen was annealed for 432 ksec at the respective temperature

Specimen	Annealing temperature (K)	x_{Sn} (at %)	c (μm)	V_{Nb_3Sn}	V_{Nb}	V_{Cu-Sn}
S1	973	0.21	1.21	0.178	0.152	0.362
	1073	0.10	1.51	0.206	0.147	0.356
S2	973	2.95	2.00	0.0982	0.219	0.375
	1073	0.54	3.85	0.176	0.158	0.359
S3	973	6.28	2.92	0.0612	0.246	0.385
	1073	2.57	6.61	0.122	0.202	0.368

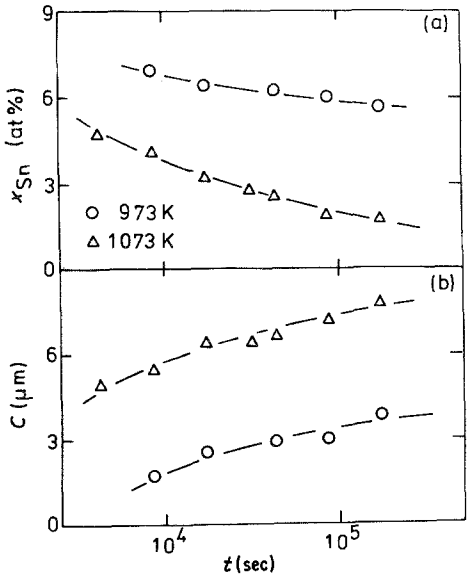

Figure 3 Variations of (a) x_{Sn} and (b) c of the S3 specimens annealed at 973 and 1073 K as a function of t.

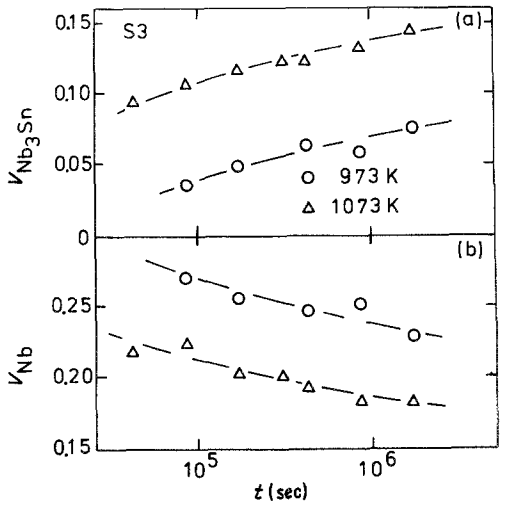

Figure 4 Variations of (a) V_{Nb_3Sn} and (b) V_{Nb} of the S3 specimens annealed at 973 and 1073 K as a function of t.

1073 K showed this type. The elongation-to-fracture of specimens showing type I mode was much higher than that of specimens showing type II mode. The type II specimens fractured in a brittle manner at low elongations. It is interesting that the strain hardening of composites as a whole in the plastic deformation stage was different in the samples belonging to type I. It was high in the S3 specimens annealed at 973 K but low in the S2 specimens annealed at the same temperature.

Fig. 6 shows the average tensile strength, σ_c, and elongation to fracture, e_c, plotted against d_c. There is a tendency for e_c to increase with increasing d_c. The variation of e_c indicates that the fracture type tends to change from type II to type I with increasing d_c at both annealing temperatures.

In order to determine the fracture mode of the Nb_3Sn layer on niobium filaments, the copper, niobium barrier, together with the Nb_3Sn layer formed at the niobium barrier and Cu–Sn, were etched away and the appearance of a Nb_3Sn layer on niobium filaments in the fractured composites was examined with the SEM. The fracture modes of Nb_3Sn layer in type I specimens were quite different from that in type II specimens. Fig. 7 shows the appearance of the Nb_3Sn layer in (a) type I and (b) type II specimens. The Nb_3Sn layer showed multiple fracture in type I but not in type II. This suggests that in type I specimens, plastic deformation of ductile constituents of copper, Cu–Sn and niobium occurred accompanying multiple fracture of the Nb_3Sn layer. Although it was found that type II specimens showed no multiple fracture of the Nb_3Sn layer, it was questionable at this stage whether any of the Nb_3Sn layer had fractured before the fracture of composite as a whole. To answer this question, the appearance of the Nb_3Sn layer in fractured type II specimens was examined over a wide area. It was found that a small number of fractures of the Nb_3Sn layer was observed, as shown in Fig. 8. This result indicates that almost all the Nb_3Sn fractured at the fracture of composites as a whole, after a small number of Nb_3Sn fractures. Next, in order to determine when multiple fracture of Nb_3Sn layer occurs in type I specimens, the appearance of this

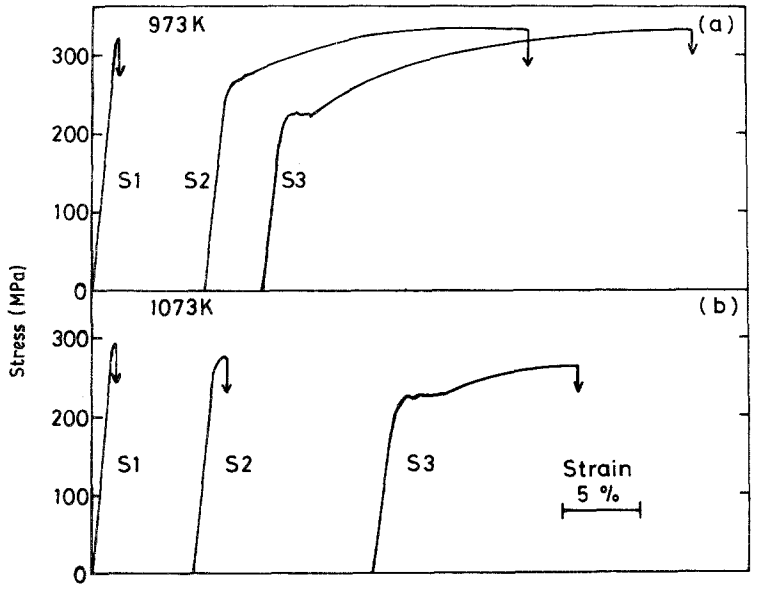

Figure 5 Typical stress–strain curves of the S1 to S3 specimens annealed at (a) 973 and (b) 1073 K for 432 ksec.

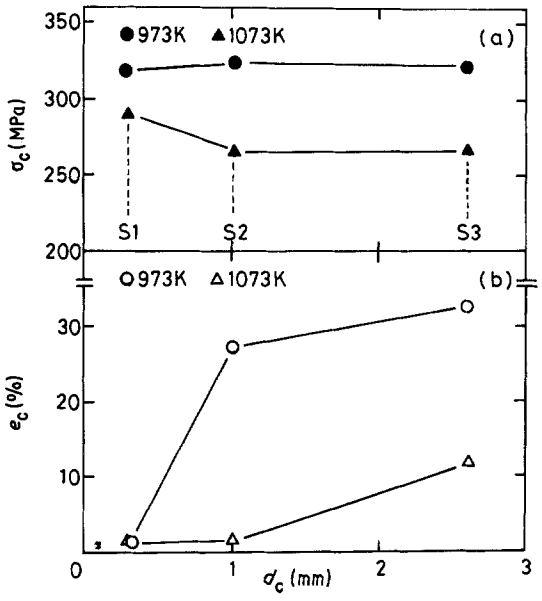

Figure 6 Measured values of (a) σ_c and (b) e_c of the S1 to S3 specimens annealed at 973 and 1073 K for 432 ksec plotted against d_c.

layer was examined after loading to various strains. Fig. 9 shows an example of the examination, where (b), (c) and (d) correspond to the strains 1, 2 and 3 shown in the stress–strain curve (a). The multiple fracture begins to occur just at the initiation of the apparent plastic deformation. Type I specimens also showed the same phenomenon. From these observations, it became evident that the apparent plastic deformation is caused by the multiple fracture of the Nb_3Sn layer.

3.2.2. Experiment 2

Within the range investigated, all the S3 specimens showed type I mode. Fig. 10 shows the variations of σ_c of the S3 specimens annealed at 973 and 1073 K as a function of t. The average lengths of segments of the Nb_3Sn layer after fracture of the composites as a whole, l_{av} together with the standard deviation, were measured as shown in Fig. 11. The l_{av} increased with increasing t at both 973 and 1073 K annealing.

4. Discussion

4.1. Features of the fracture modes of types I and II

As shown in Section 3.2, there are two distinct types, I and II, in the deformation and fracture behaviour of composites. The features of each type could be summarized as follows.

1. Type I

(i) Apparent plastic deformation of composites as a whole is found and accordingly e_c is high.

(ii) The Nb_3Sn layer shows multiple fracture.

(iii) The multiple fracture of the Nb_3Sn layer begins just at the initiation of apparent plastic deformation of composites as a whole.

2. Type II

(i) No apparent plastic deformation of composites as a whole is found and accordingly e_c is low. The specimens fracture in a brittle manner.

(ii) The Nb_3Sn layer does not show multiple fracture. Before fracture of composites, a small number of breakages of the Nb_3Sn layer occur and most of the Nb_3Sn layer fractures at the fracture of composites.

The features of type I indicate that the drop of load-bearing capacity of composites as a whole due to breakage of the Nb_3Sn layer can be compensated by work hardening of ductile constituents of copper, Cu–Sn and niobium and the stress can be transferred to the once-fractured Nb_3Sn layer, which can be again fractured into shorter lengths [9, 10]. On the other

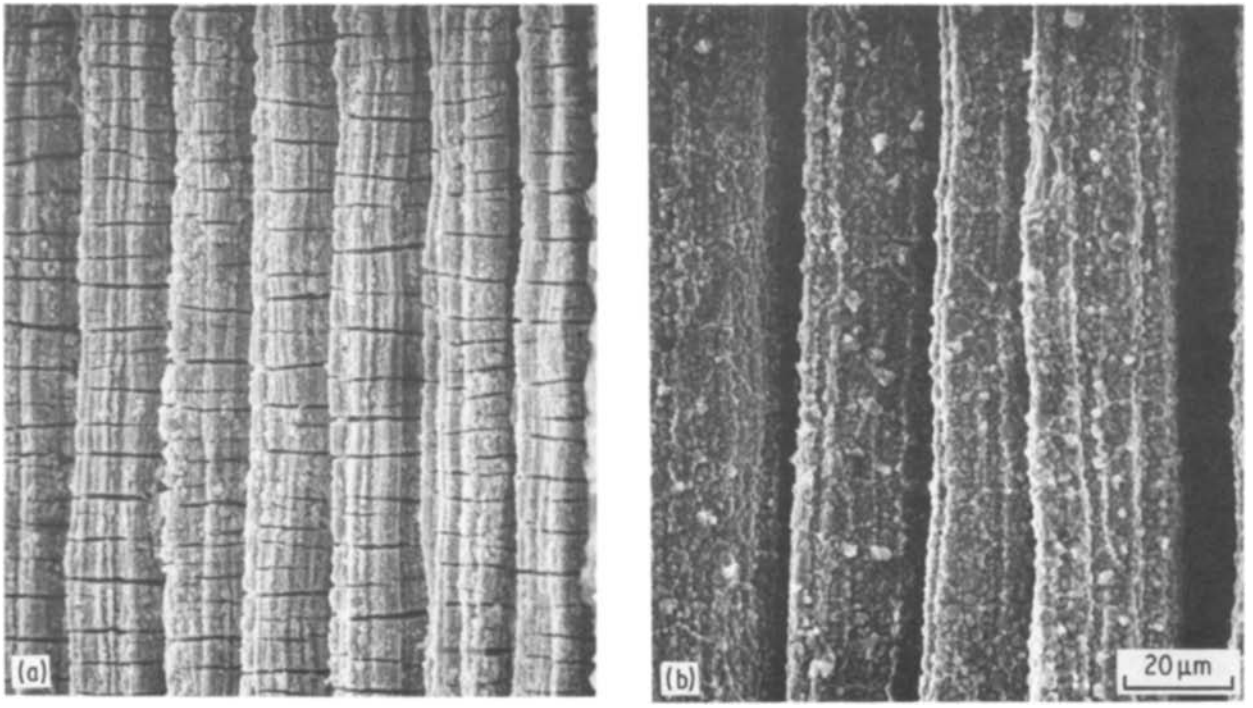

Figure 7 Appearance of the Nb_3Sn layer after fracture of the specimens as a whole. (a) Multiple fracture of the Nb_3Sn layer, observed in the S2 specimen annealed at 973 K for 432 ksec, which showed type I fracture mode. (b) No multiple fracture of the layer, observed in the S2 specimen annealed at 1073 K for 432 ksec, whcih showed type II fracture mode.

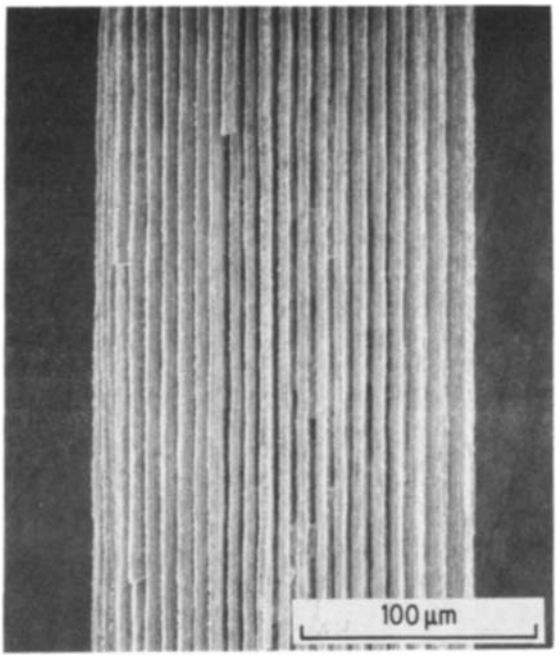

Figure 8 Macroscopic view of the appearance of the Nb_3Sn layer after fracture of the S1 specimen annealed at 973 K for 432 ksec, which showed type II fracture mode.

hand, the features of type II indicate that, essentially, the fracture of Nb_3Sn layer causes the fracture of composites as a whole. This fracture mode has often been observed in fibre-reinforced metal matrix composites [11–14]. In this type, the fracture of composites as a whole occurs when a small number of fibres break, followed by a chain reaction of fracture of the remaining fibres [11–14]. In the present specimens, the Nb_3Sn layer can be regarded as fibres in fibre-reinforced composites. In the present specimens, if, after a small number of breakages of the Nb_3Sn layer, the chain reaction of breakages of the Nb_3Sn layer could not occur due to work hardening of the ductile constituents, the Nb_3Sn layer would show multiple fracture, as observed in the specimens showing type I. Thus the stress at which multiple fracture of the Nb_3Sn layer begins in type I can be regarded as the stress at which composites would fracture in type II.

4.2. A proposed model to describe tensile strength of composites

In order to describe the tensile strength of composites and to explain the reason why some specimens show type I while others show type II, the following model is proposed.

Denoting the stress of composites at which multiple fracture of the Nb_3Sn layer begins in type I, which corresponds to the fracture stress for type II, as σ_c^A, the σ_c^A is realized at low strains, being nearly equal to the average fracture strain of the Nb_3Sn layer (less than $\sim 1\%$ in the present specimens as shown later). At such low strains, the stresses borne by the ductile constituents of copper, Cu–Sn and niobium are low compared with the respective tensile strength, since they show their full strength after high strains such as 30 to 50%. Thus it is possible that work hardening of the ductile constituents can compensate the drop of stress due to breakage of Nb_3Sn layer in type I, while it is impossible in type II. Thus for type I mode, one can predict an existence of the maximum stress of composites, which is borne mainly by the ductile constituents and partially by the segmented Nb_3Sn layer after high plastic deformation. Defining this maximum stress as σ_c^B, the σ_c^B gives the tensile strength of the composites for type I. For the case of $\sigma_c^A < \sigma_c^B$, the Nb_3Sn layer begins to fracture at the stress corresponding to σ_c^A, but beyond this stress, composites can deform further, since a drop of stress due to fracture of the Nb_3Sn layer can be compensated. In this case, as stress is transferred to the once-broken Nb_3Sn layer, the Nb_3Sn layer shows multiple fracture. This case corresponds to type I. On the other hand, in the case of $\sigma_c^A > \sigma_c^B$, the highest stress is realized at the stress of σ_c^A, since the drop of stress due to fracture of Nb_3Sn cannot be compensated. Thus the composite fractures at the stress of σ_c^A without further plastic deformation beyond σ_c^A. This case corresponds to type II, and the strength of composites is given by σ_c^A.

4.2.1. Estimation of σ_c^A

σ_c^A can be given approximately by the rule of mixtures [9, 15] in the form

$$\sigma_c^A = \sigma_{Nb_3Sn} V_{Nb_3Sn} + \sigma^*_{Cu} V_{Cu} + \sigma^*_{Cu-Sn} V_{Cu-Sn} + \sigma^*_{Nb} V_{Nb} \quad (1)$$

where the σ_{Nb_3Sn} is the stress borne by the Nb_3Sn layer, the σ^* is the stress borne by the constituents other than the Nb_3Sn layer at the initiation of the multiple fracture of the layer for type I and at the fracture of composites for type II, and V is the respective volume fraction. The rigid estimation of σ^* is difficult in the present specimens due to residual stresses arising from the difference in thermal contractions among the constituents, which are introduced during cooling from the annealing temperatures. Then, in the present study, σ^* will be given approximately as follows.

In composites annealed to form the Nb_3Sn layer and then cooled to room temperature, the Nb_3Sn and niobium are subjected to compressive residual stresses and the copper and Cu–Sn to tensile residual stresses. Sometimes, the copper and Cu–Sn have yielded in the longitudinal direction [16]. Fig. 12 shows a schematic representation of the stress–strain curves of composites and each constituent under tensile loading. The stresses of the constituents at zero strain show the residual stresses. In Fig. 12, the case where copper and Cu–Sn have already yielded during cooling is drawn as an example. The $\sigma_{Cu,y}$ and $\sigma_{Cu-Sn,y}$ show the yield stresses of copper and Cu–Sn, respectively, and the σ^r_{Nb} and $\sigma^r_{Nb_3Sn}$ the residual (compressive) stresses in niobium and Nb_3Sn layer, respectively. Generally, the stresses of σ^*_{Cu} and σ^*_{Cu-Sn} are not so much different from the respective yield stress in the range of low strain, as in the present composites. When the Cu–Sn is annealed fully, as in the present experiment, yield stress, σ_y, tensile strength, σ_u, and elongation, e, are given as a function of x_{Sn}, as shown in Fig. 13, whose data points were taken from [17]. As x_{Sn} was measured for each annealing treatment, the σ^*_{Cu-Sn} can be read from the yield stress–x_{Sn} relation shown in Fig. 13 by

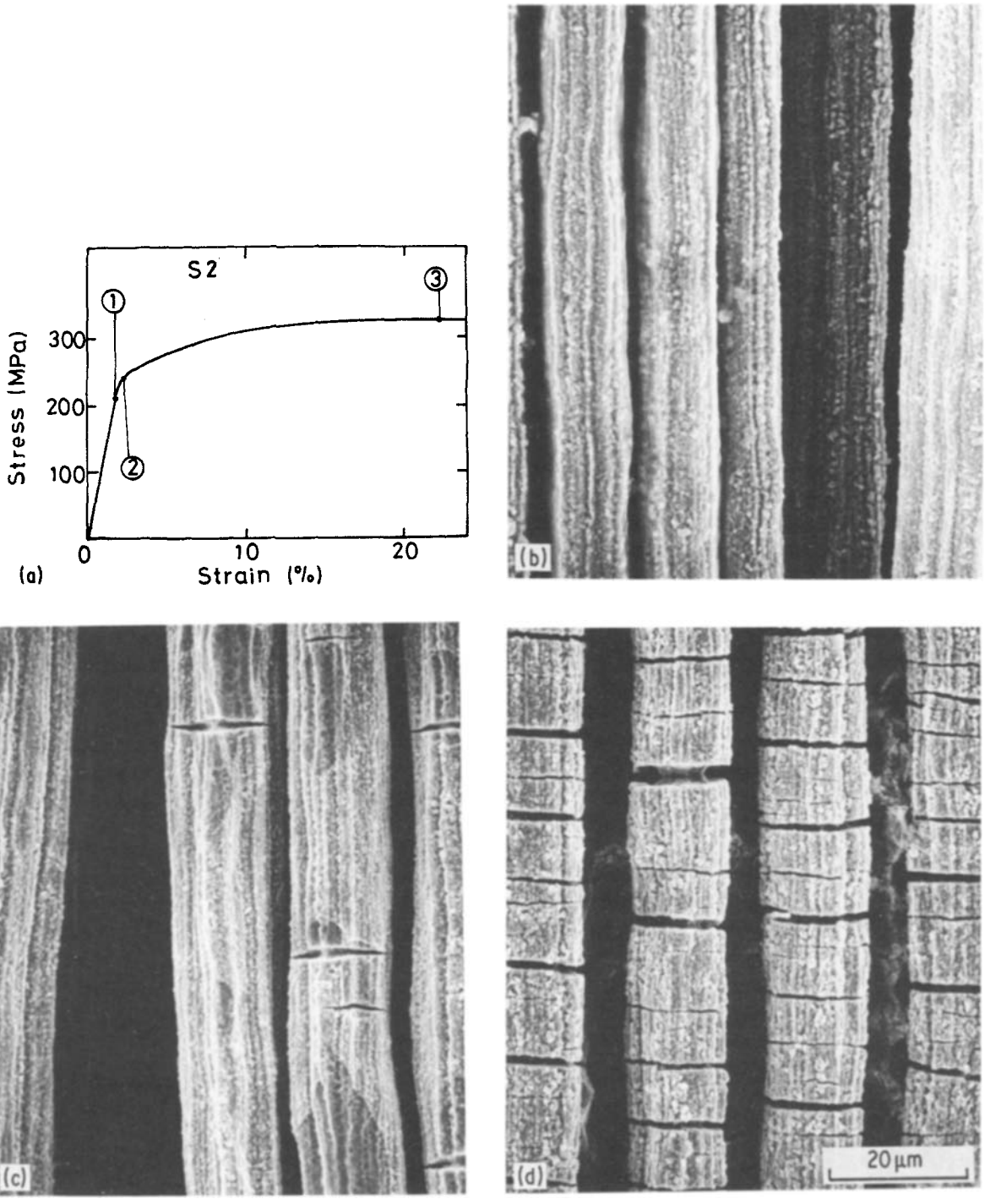

Figure 9 Appearance of the Nb_3Sn layer at the strains indicated in the stress–strain curve of the S2 specimens annealed at 973 K for 432 ksec, which showed type I fracture mode.

interpolating the x_{Sn} for each annealing treatment. The σ^*_{Cu} was taken from the yield stress for $x_{Sn} = 0$ in Fig. 13. The behaviour of niobium filaments and the niobium barrier were difficult to measure separately in this work, therefore it was assumed that the niobium filaments and the niobium barrier behave similarly under the same heat-treatment. In order to determine the mechanical properties of niobium the niobium filaments with a diameter of 0.65 mm, supplied by Sumitomo Electric Industries Ltd (Osaka, Japan), were annealed at 973 and 1073 K for various times and then tensile-tested. As it was found that the time-dependency of the yield stress and tensile strength of the niobium filaments is small at each temperature, the average measured values of them were used in the calculation. The average values of yield stress, tensile strength and strain to fracture were 233 MPa, 383 MPa and 27% for the annealing at 973 K, respectively, and 221 MPa, 357 MPa and 27% for annealing at 1073 K, respectively. Then 233 MPa at 973 K annealing and 221 MPa at 1073 K annealing were used as σ^*_{Nb}. The above measured values were also used in the calculation of σ^B_c.

4.2.2. Estimation of σ^B_c

The strength of composites which shows high plastic deformation accompanying with multiple fracture of the Nb_3Sn layer, σ^B_c, may be expressed as

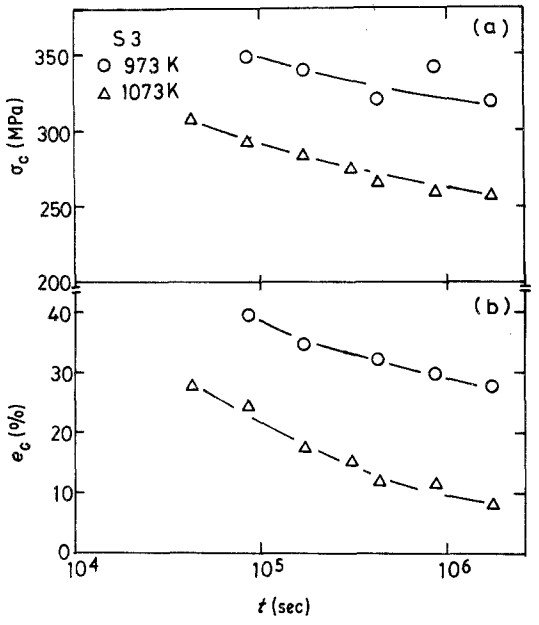

Figure 10 Variations of (a) σ_c and (b) e_c of the S3 specimens annealed at 973 and 1073 K as a function of t.

$$\sigma_c^B = \sigma_{Cu,Cu-Sn,Nb} V_{Cu,Cu-Sn,Nb} + \sigma'_{Nb_3Sn} V_{Nb_3Sn} \quad (2)$$

where $\sigma_{Cu,Cu-Sn,Nb}$ is the stress capacity of the ductile constituents, $V_{Cu,Cu-Sn,Nb}$ is the sum of the volume fractions of Cu, Cu–Sn and Nb, and the σ'_{Nb_3Sn} is the contribution of the Nb_3Sn layer after multiple fracture. A rough estimation of $\sigma_{Cu,Cu-Sn,Nb}$ can be made by modifying the theory, which describes the tensile instability of metal fibre-reinforced metal matrix composites [18–20]. Assuming the true stress, σ, and true plastic strain, ε, curve is expressed in the form

$$\sigma = (a + b\varepsilon)^n \quad (3)$$

where a, b and n are constants, the yield stress, tensile strength and true strain to fracture correspond to a^n, $(nb)^n$ and $(nb\text{-}a)/b$, respectively. For copper, Cu–Sn and niobium, the values of a, b and n can be calculated by using the data shown already. If it were not for the Nb_3Sn layer, the normal stress of ductile constituents at $\varepsilon = \varepsilon$, $\sigma^n_{Cu,Cu-Sn,Nb}$, is given by

$$\sigma^n_{Cu,Cu-Sn,Nb} = [(a_{Cu} + b_{Cu}\varepsilon)^{n_{Cu}} V'_{Cu} + (a_{Cu-Sn} + b_{Cu-Sn}\varepsilon)^{n_{Cu-Sn}} V'_{Cu-Sn} + (a_{Nb} + b_{Nb}\varepsilon)^{n_{Nb}} V'_{Nb}] \exp(-\varepsilon) \quad (4)$$

where V'_{Cu}, V'_{Cu-Sn} and V'_{Nb} are given by $V_{Cu}/V_{Cu,Cu-Sn,Nb}$, $V_{Cu-Sn}/V_{Cu,Cu-Sn,Nb}$ and $V_{Nb}/V_{Cu,Cu-Sn,Nb}$, respectively. Noting the normal strain as e, which has a relationship to ε as $\varepsilon = \ln(1 + e)$, the maximum stress of $\sigma^n_{Cu,Cu-Sn,Nb}$, which is the stress capacity of ductile constituents as a whole, satisfies Equation 5:

$$d\sigma^n_{Cu,Cu-Sn,Nb}/de = 0 \quad (5)$$

Combining Equations 4 and 5 one can calculate the value of $\sigma_{Cu,Cu-Sn,Nb}$. This calculated value corresponds

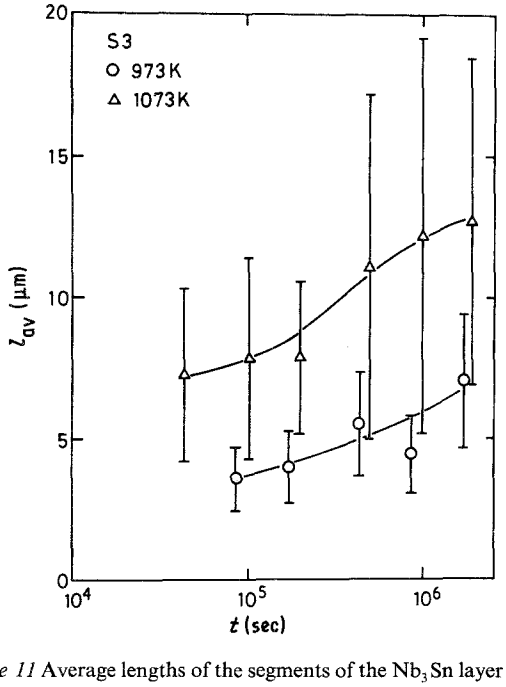

Figure 11 Average lengths of the segments of the Nb_3Sn layer in the fractured S3 specimens annealed at 973 and 1073 K.

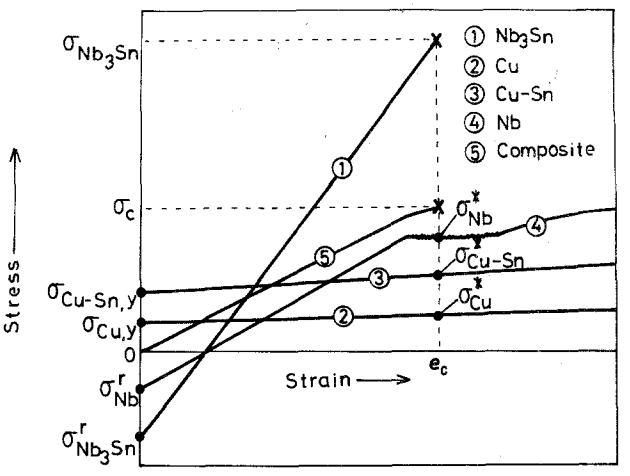

Figure 12 Schematic representation of the stress–strain curves of each constituent and the composite as a whole for the type II fracture mode.

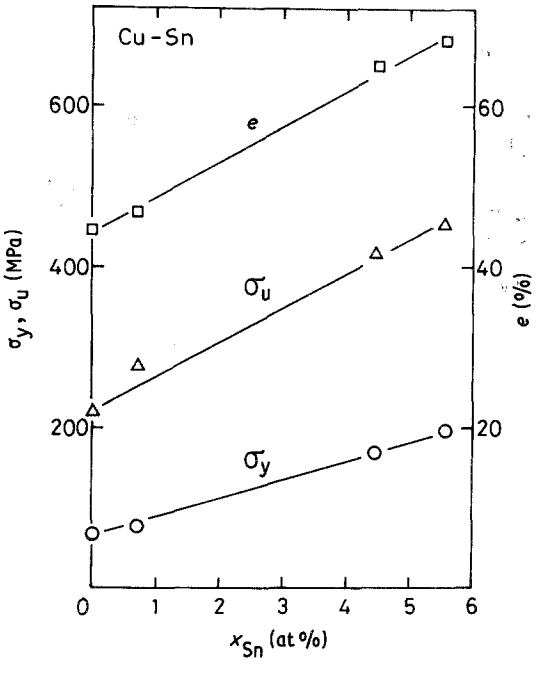

Figure 13 Variations of yield stress σ_y, tensile strength, σ_u and fracture strain e of the Cu–Sn alloy as a function of x_{Sn}, where data points were taken from [17].

to the strength which could be realized if the Nb_3Sn layer did not exist: namely it could be realized at the imaginary cross-section where all Nb_3Sn layers have broken. However, not only the ductile constituents but also the Nb_3Sn layer can support the applied load in real composites, since the Nb_3Sn layer exists in any cross-section, in which applied stress can be transferred to the Nb_3Sn layer even if the layer has been segmented. The stress supported by the segmented Nb_3Sn layer can be estimated by modifying the Kelly–Tyson model [9], which was originally proposed to describe the stress distribution in discontinuous fibres in metal matrix composites. In a segment of the Nb_3Sn layer with a length l, cross-sectional area A and thickness c, on a niobium filament with a diameter d_f, the stress in the segment from the end, $\sigma_{Nb_3Sn}(x)$, where x is the distance from the end, is approximately given by

$$\sigma_{Nb_3Sn}(x) = \{\pi d_f \tau_{Nb} + \pi(d_f + 2c)\tau_{Cu-Sn}\}x/A \quad (6)$$

where τ_{Nb} and τ_{Cu-Sn} are the shear stresses of niobium and Cu–Sn alloy, respectively, which are approximately given by the halves of the tensile yield stresses of niobium and Cu–Sn, respectively. The average stress supported by the Nb_3Sn segment is then given by

$$\sigma'_{Nb_3Sn} = (l/4A)[\pi d_f \tau_{Nb} + \pi(d_f + 2c)\tau_{Cu-Sn}] \quad (7)$$

Substituting the calculated values of $\sigma_{Cu,Cu-Sn,Nb}$ and σ'_{Nb_3Sn} into Equation 2 one can find the value of σ_c^B.

4.3. Application of the proposed model to the experimental results

4.3.1. Experiment 1

The proposed model was first applied to the results of Experiment 1, where the S1 specimens annealed at 973 K and the S1 and S2 specimens annealed at 1073 K showed type II while the S2 and S3 specimens annealed at 973 K and the S3 specimens annealed at 1073 K showed type I.

First, σ_c^B was calculated for the specimens which showed type I where the measured average values of l were 6.67, 5.55 and 11.1 μm in the S2(973 K), S3(973 K), and S3(1073 K) specimens, respectively. Table II shows the comparison of the calculated values with the measured ones, together with the measured values of σ_c^A. The σ_c^B(i) is the value calculated by Equation 2 and the σ_c^B(ii) is the value of $\sigma_{Cu,Cu-Sn,Nb} V_{Cu,Cu-Sn,Nb}$ where the contribution of $\sigma_{Nb_3Sn} V_{Nb_3Sn}$ to σ_c^B in Equation 2 is neglected. The calculated values of σ_c^B(i) and σ_c^B(ii) agree fairly well with the measured ones. In these specimens, the contribution of $\sigma'_{Nb_3Sn} V_{Nb_3Sn}$ to σ_c^B is small compared with that of $\sigma_{Cu,Cu-Sn,Nb} V_{Cu,Cu-Sn,Nb}$. In the specimens showing type I, the values of σ_c^B are higher than those of σ_c^A, as expected. Fig. 14 shows the variation of σ_c^B as a function of d_c, in which the σ_c^B(ii) is taken as σ_c^B, together with the variation of σ_c^A. For the S1(973 K), S1(1073 K) and S2(1073 K) specimens, which showed type II mode, the σ_c^B is lower than σ_c^A, but for the S2(973 K), S3(973 K) and S3(1073 K) specimens, which showed type I mode, the σ_c^B is higher than σ_c^A. Thus the reason why the former specimens fractured in a brittle manner without apparent plastic deformation of composites as a whole and why the latter specimens showed apparent plastic deformation accompanying multiple fracture of the Nb_3Sn layer, is well understood.

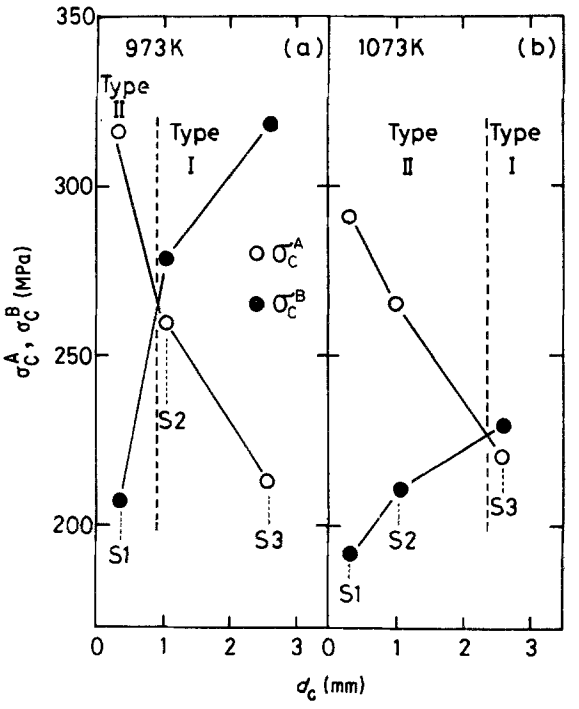

Figure 14 Comparison of the calculated values of σ_c^B with the measured values of σ_c^A in the S1 to S3 specimens annealed at 973 and 1073 K for 432 ksec.

4.3.2. Experiment 2

The σ_c^B(i) and σ_c^B(ii) were also calculated for the S3 specimens annealed for various times, all of which

TABLE II Measured and calculated values of σ_c^A and σ_c^B of the S1 to S3 specimens annealed at 973 and 1073 K for 432 ksec

Specimen	Annealing temperature (K)	Fracture type	$\sigma^A_{c,mea}$ (MPa)	$\sigma^B_{c,mea}$ (MPa)	$\sigma^B_{c,cal}$ (i) (MPa)*	$\sigma^B_{c,cal}$ (ii) (MPa)†
S1	973	II	321	–	–	207
	1073	II	295	–	–	191
S2	973	I	259	323	295	279
	1073	II	266	–	–	210
S3	973	I	230	321	337	331
	1073	I	222	262	267	259

*$\sigma^B_{c,cal}$(i) = $\sigma_{Cu,Cu-Sn,Nb} V_{Cu,Cu-Sn,Nb} + \sigma'_{Nb_3Sn} V_{Nb_3Sn}$

†$\sigma^B_{c,cal}$(ii) = $\sigma_{Cu,Cu-Sn,Nb} V_{Cu,Cu-Sn,Nb}$

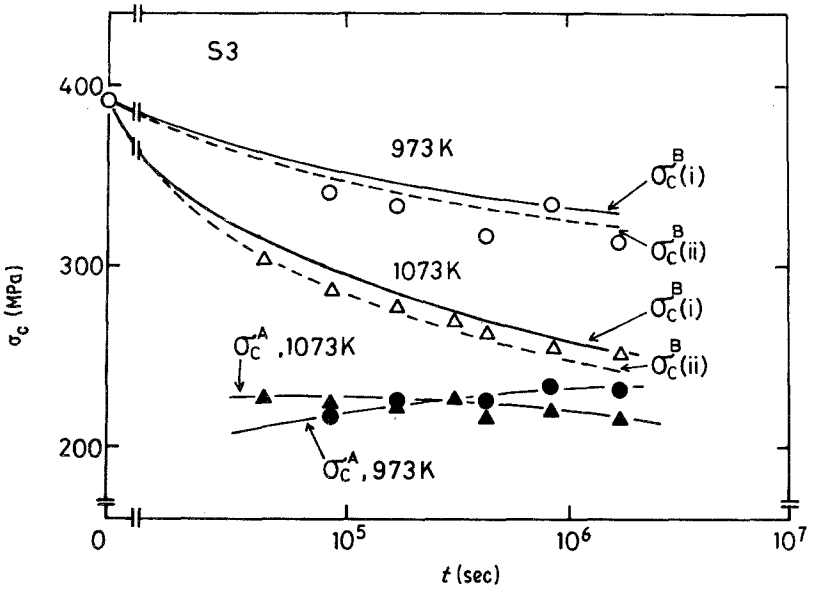

Figure 15 Comparison of the measured values of σ_c with the calculated values of σ_c^B of the S3 specimens isothermally annealed at 973 and 1073 K.

showed type I. The results are shown in Fig. 15. The calculated values of σ_c^B agree well with the measured values of tensile strength of composites.

In the S3 specimens annealed for various times, type II fracture mode was not observed within the range investigated. However, in experiment 1, the S1 specimens exhibited type II fracture mode when annealed at 973 and 1073 K for 432 k sec. In these specimens, the σ_c^A was higher than σ_c^B in the calculation as already shown in Table II. The S1 specimens could, however, show type I fracture mode if a situation of $\sigma_c^B > \sigma_c^A$ could be realized. As σ_c^B is expected to decrease with increasing annealing time, when isothermally annealed, due to decrease of V_{Nb}, x_{Sn} which determines strength of Cu–Sn, and V_{Cu-Sn} and due to increase in V_{Nb_3Sn}, the S1 specimens are expected to show type I mode for short annealing time. To examine this speculation, the S1 specimens were annealed isothermally at 973 K and then tensile-tested. As speculated, the fracture mode changed from type I to type II with increasing annealing time. Fig. 16 shows the variation of e_c plotted against t and the regions of time for types I and II. In this experiment, the type I mode was observed for $t \leqq 173$ k sec but type II for $t \geqq 432$ k sec. In the range of $t \leqq 173$ k sec where

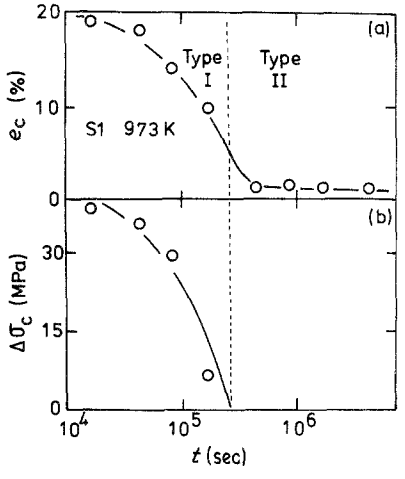

Figure 16 Variation of e_c of the S1 specimens annealed at (a) 973 K and (b) variation of $\Delta\sigma_c$ for type I as a function of t.

type I was observed, the difference between the measured values of σ_c^B and σ_c^A, $\Delta\sigma_c$, decreased with increasing t as shown in Fig. 16b. Extrapolating the $\Delta\sigma_c$–t curve to the point of $\Delta\sigma_c = 0$, the transition time from type I to II was roughly read to be 3×10^5 sec, which corresponds to the time where e_c decreased abruptly in the e_c–t curve.

4.4. Tensile strength of the Nb_3Sn layer

The measured values of σ_c^A together with the values of V and σ^* of each component in Equation 1, and the values of σ_{Nb_3Sn} were calculated. As σ_{Nb_3Sn} is the stress of the Nb_3Sn layer at which multiple fracture arises for type I, and that at which composites fracture as a whole for type II, it is not necessarily the same as the average tensile strength. In the case of fibre-reinforced metal, the fibre stress at which composites fracture is, in general, lower than the average strength of fibre, according to the computer simulation [21]. However, the difference is not so much (less than 20% at most) as long as interfacial bonding strength between the fibre and matrix is high enough to supress debonding at the interface and the shear yield stress of matrix is higher than 35 MPa, as in the present specimens [21]. Therefore, the σ_{Nb_3Sn} can be regarded as the average tensile strength of the Nb_3Sn layer to a first approximation. The calculated values of σ_{Nb_3Sn} are shown in Fig. 17. It is clearly shown that the σ_{Nb_3Sn} decreases with increasing d_c and also with increasing annealing temperature and time. This suggests that thin composites annealed at low temperatures for short times can realize a high strength of the Nb_3Sn layer. Taking the Young's modulus of the Nb_3Sn layer as 165 GPa [1], the fracture strain of this layer is 0.5% to 1% in the present specimens.

5. Conclusions

The structure and tensile behaviour of the Nb_3Sn superconducting composite materials were studied. Two types of fracture mode were observed. When the amount of the Nb_3Sn was small, the drop of load-bearing capacity due to breakage of the Nb_3Sn layer could be compensated mainly by the strain hardening

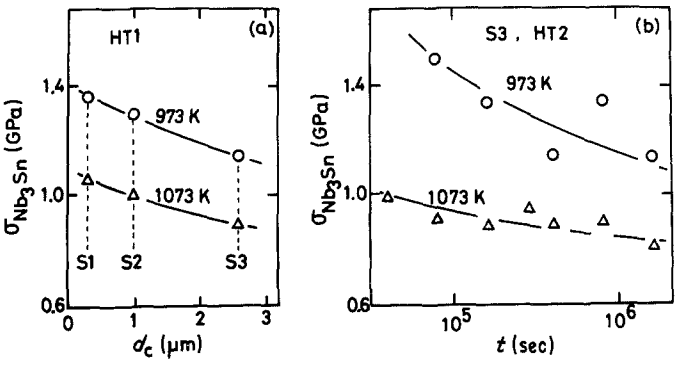

Figure 17 Estimated values of σ_{Nb_3Sn} layer of (a) the S1 to S3 specimens annealed at 973 and 1073 K for 432 ksec plotted against d_c, and (b) those of the S3 specimens annealed at 973 and 1073 K plotted against t.

of ductile constituents, and the composites showed high strain to fracture. In this type, the Nb_3Sn layer exhibited multiple fracture. On the contrary, when the amount of the Nb_3Sn is large, the fracture of composites was caused by a small number of breakages of the Nb_3Sn layer and the composites fractured in a brittle manner. In this type, the strain of composites to fracture was very low compared to that in the other type. To describe the tensile strength for both types, a model was proposed, which explained the experimental results well. The strength of the Nb_3Sn layer, estimated on the basis of the rule of mixtures, showed a tendency to decrease with diameter of the specimens and with increasing annealing temperature and time.

Acknowledgements

The authors wish to thank Messrs I. Nakagawa and T. Unesaki at Kyoto University for their help in the SEM and EPMA studies, and Messrs M. Nagata and S. Okuda at Sumitomo Electric Industries Ltd for their helpful comments. They also thank The Ministry of Education, Science and Culture of Japan for the grant-in-aid for developmental scientific research (no. 58850155).

References

1. J. W. EKIN in "Superconducting Materials Science-Metallurgy, Fabrication and Applications", edited by S. Foner and B. B. Schwarz (Plenum, New York, 1981) p. 455.
2. L. R. TESTARDI *Phys. Rev.* **B3** (1971) 95.
3. C. C. KOCK and D. S. EASTON, *Cryogenics* **17** (1977) 391.
4. J. W. EKIN, *ibid.* **20** (1980) 611.
5. E. J. KRAMER, *J. Appl. Phys.* **44** (1973) 1360.
6. T. LUHMAN, M. SUENAGA, D. O. WELCH and K. KAIHO, *IEEE Trans. Ma.* **MAG-15** (1979) 699.
7. T. LUHMAN, *J. Appl. Phys.* **50** (1979) 3766.
8. T. LUHMAN, M. SUENAGA and C. J. KLAMUT, *Adv. Cryo. Eng.* **24** (1978) 325.
9. A. KELLY and W. R. TYSON, *J. Mech. Phys. Solids* **13** (1965) 329.
10. S. OCHIAI, M. MIZUHARA, K. SHIMOMURA and Y. MURAKAMI, *Trans. Jpn. Inst. Metals* **16** (1975) 345.
11. C. ZWEBEN, *AIAA J.* **6** (1968) 2325.
12. C. ZWEBEN and B. W. ROSEN, *J. Mech. Phys. Solids* **18** (1970) 189.
13. H. W. HERRING, J. L. LYTTON and J. H. STEELE Jr, *Met. Trans.* **4** (1973) 807.
14. S. OCHIAI, K. OSAMURA and K. ABE, *Z. Metallkde* **76** (1985) 402.
15. D. L. McDANELS, R. W. JECH and J. W. WEETON, *Trans. Met. Soc. AIME* **223** (1965) 636.
16. D. S. EASTON, D. M. KROEGER, W. SPECKING and C. C. KOCH, *J. Appl. Phys.* **51** (1980) 2748.
17. ASM Committee on Copper and Copper Alloys: "Metals Handbook", Vol. 2, Properties and Selections: Nonferrous Alloys and Pure Metals (American Society for Metals, Metals Park, Ohio, 1979) p. 275.
18. S. T. MILEIKO, *J. Mater. Sci.* **4** (1969) 974.
19. G. GARMONG and R. B. THOMPSON, *Met. Trans.* **4** (1973) 863.
20. S. OCHIAI and Y. MURAKAMI, *J. Mater. Sci.* **15** (1980) 1798.
21. S. OCHIAI and K. OSAMURA, *Z. Metallkde* **76** (1985) 485.

Received 12 April
and accepted 30 May 1985